



**AFRL-RY-WP-TR-2012-0167**

**NANOPHOTONIC SENSOR INTEGRATION AND  
COHERENT FEEDBACK**

**Professor Hideo Mabuchi**

**Leland Stanford Junior University**

**FEBRUARY 2012  
Final Report**

**Approved for public release; distribution unlimited.**

*See additional restrictions described on inside pages*

**STINFO COPY**

**AIR FORCE RESEARCH LABORATORY  
SENSORS DIRECTORATE  
WRIGHT-PATTERSON AIR FORCE BASE, OH 45433-7320  
AIR FORCE MATERIEL COMMAND  
UNITED STATES AIR FORCE**

## NOTICE AND SIGNATURE PAGE

Using Government drawings, specifications, or other data included in this document for any purpose other than Government procurement does not in any way obligate the U.S. Government. The fact that the Government formulated or supplied the drawings, specifications, or other data does not license the holder or any other person or corporation; or convey any rights or permission to manufacture, use, or sell any patented invention that may relate to them.

This report was cleared for public release by the Wright-Patterson Public Affairs Office and is available to the general public, including foreign nationals. Copies may be obtained from the Defense Technical Information Center (DTIC) (<http://www.dtic.mil>).

AFRL-RY-WP-TR-2012-0167 HAS BEEN REVIEWED AND IS APPROVED FOR PUBLICATION IN ACCORDANCE WITH THE ASSIGNED DISTRIBUTION STATEMENT.

*\*/signature/*

---

VASSILIOS KOVANIS, Project Manager  
Electro-Optic Components Branch  
Aerospace Components Division

*//signature/*

---

THOMAS R. NELSON, Chief  
Electro-Optic Components Branch  
Aerospace Components Division

*//signature/*

---

BRADLEY CHRISTIANSEN, Lt Col, USAF  
Deputy Division Chief  
Aerospace Components Division  
Sensors Directorate

This report is published in the interest of scientific and technical information exchange, and its publication does not constitute the Government's approval or disapproval of its ideas or findings.

\*Disseminated copies will show "*//signature/*" stamped or typed above the signature blocks.

<b>REPORT DOCUMENTATION PAGE</b>				<i>Form Approved</i> OMB No. 0704-0188	
<p>The public reporting burden for this collection of information is estimated to average 1 hour per response, including the time for reviewing instructions, searching existing data sources, gathering and maintaining the data needed, and completing and reviewing the collection of information. Send comments regarding this burden estimate or any other aspect of this collection of information, including suggestions for reducing this burden, to Department of Defense, Washington Headquarters Services, Directorate for Information Operations and Reports (0704-0188), 1215 Jefferson Davis Highway, Suite 1204, Arlington, VA 22202-4302. Respondents should be aware that notwithstanding any other provision of law, no person shall be subject to any penalty for failing to comply with a collection of information if it does not display a currently valid OMB control number. <b>PLEASE DO NOT RETURN YOUR FORM TO THE ABOVE ADDRESS.</b></p>					
<b>1. REPORT DATE (DD-MM-YY)</b> February 2012		<b>2. REPORT TYPE</b> Final		<b>3. DATES COVERED (From - To)</b> 08 October 2009 – 07 October 2011	
<b>4. TITLE AND SUBTITLE</b> NANOPHOTONIC SENSOR INTEGRATION AND COHERENT FEEDBACK				<b>5a. CONTRACT NUMBER</b> FA8650-10-1-7007	
				<b>5b. GRANT NUMBER</b>	
				<b>5c. PROGRAM ELEMENT NUMBER</b> 62716E	
<b>6. AUTHOR(S)</b> Professor Hideo Mabuchi				<b>5d. PROJECT NUMBER</b> ARPR	
				<b>5e. TASK NUMBER</b> YD	
				<b>5f. WORK UNIT NUMBER</b> ARPRYD26	
<b>7. PERFORMING ORGANIZATION NAME(S) AND ADDRESS(ES)</b>  Leland Stanford Junior University 450 Serra Mall Stanford, CA 94305				<b>8. PERFORMING ORGANIZATION REPORT NUMBER</b>	
<b>9. SPONSORING/MONITORING AGENCY NAME(S) AND ADDRESS(ES)</b>  Air Force Research Laboratory Sensors Directorate Wright-Patterson Air Force Base, OH 45433-7320 Air Force Materiel Command United States Air Force				<b>10. SPONSORING/MONITORING AGENCY ACRONYM(S)</b> AFRL/RYPD	
				<b>11. SPONSORING/MONITORING AGENCY REPORT NUMBER(S)</b> AFRL-RY-WP-TR-2012-0167	
<b>12. DISTRIBUTION/AVAILABILITY STATEMENT</b> Approved for public release; distribution unlimited.					
<b>13. SUPPLEMENTARY NOTES</b> PAO Case Number: 88ABW-2012-2743, cleared 23 May 2012. Report contains color.					
<b>14. ABSTRACT</b>  During the period of this seedling grant, we have performed experimental research on attojoule-scale absorptive optical bistability in single-atom cavity QED. Also, as well as, theoretical research on coherent feedback control of dispersive bistability and on a nonlinear interferometry approach to photonic sequential logic.					
<b>15. SUBJECT TERMS</b> nanotechnology, mid-infrared lasers, bistability, interferometry					
<b>16. SECURITY CLASSIFICATION OF:</b>			<b>17. LIMITATION OF ABSTRACT:</b> SAR	<b>18. NUMBER OF PAGES</b> 22	<b>19a. NAME OF RESPONSIBLE PERSON (Monitor)</b> Vassilios Kovanis <b>19b. TELEPHONE NUMBER (Include Area Code)</b> N/A
<b>a. REPORT</b> Unclassified	<b>b. ABSTRACT</b> Unclassified	<b>c. THIS PAGE</b> Unclassified			

## TABLE OF CONTENTS

Section	Page
List of Figures.....	ii
1.0 SUMMARY.....	1
2.0 COHERENT-FEEDBACK CONTROL OF OPTICAL BISTABILITY.....	1
3.0 NONLINEAR INTERFEROMETRY APPROACH TO PHOTONIC LOGIC... 4	
4.0 QUANTUM REMNANTS OF BISTABILITY IN THE ATTOJOULE REGIME 8	

## LIST OF FIGURES

<b>Figure</b>		<b>Page</b>
1	Quantum trajectory simulation.....	2
2	Coherent feedback schemes.....	3
3	Effects of coherent feedback.....	3
4	Change in spontaneous switching rates.....	4
5	Diagrams of AND, NOT gates.....	5
6	Kerr nonlinearities.....	6
7	Bistable latch diagram.....	7
8	Bistable behavior.....	8
9	Absorptive bistability in cavity QED.....	10
10	Steady-state homodyne distributions.....	11
11	Correlation functions.....	12
12	Hysteresis results.....	13

## 1.0 SUMMARY

An optical resonator with intracavity Kerr nonlinearity can exhibit dispersive bistability suitable for all-optical switching. With nanophotonic elements it may be possible to achieve attojoule switching energies, which would be very attractive for ultra-low power operation but potentially problematic because of quantum fluctuation-induced spontaneous switching. We derive a quantum-optical model of two Kerr-nonlinear ring resonators connected in a coherent feedback loop, and show via numerical simulation that a properly designed “controller” cavity can significantly reduce the spontaneous switching rate of a bistable “plant” cavity in a completely embedded and autonomous manner. Motivated by rapidly advancing capabilities for extensive nanoscale patterning of optical materials, we also propose an approach to implementing photonic sequential logic that exploits circuit-scale phase coherence for efficient realizations of fundamental components such as a NAND-gate-with-fanout and a bistable latch. Kerr-nonlinear optical resonators are utilized in combination with interference effects to drive the binary logic. Quantum-optical input-output models are characterized numerically using design parameters that yield attojoule-scale energy separation between the latch states.

## 2.0 COHERENT-FEEDBACK CONTROL OF OPTICAL BISTABILITY

Although current nanophotonics research focuses mainly on the design and demonstration of individual optical components, future progress towards technological relevance will surely require the development of nanophotonic circuit theory at a level of sophistication comparable to that of modern electronics. As the performance regime of interest for nanophotonic technologies extends to picosecond switching times and attojoule (few-photon) switching energies, quantum-optical effects will be of great practical significance even if the information processing paradigm remains purely classical (i.e., before the advent of true quantum information technology). Rigorous yet user-friendly theoretical methods (based on generalizations of classical stochastic systems theory) for the quantum-optical analysis of photonic circuits have recently been developed, but compatible algorithmic design methods are still quite limited in scope. It is thus an opportune moment to begin investigating relatively simple nanophotonic circuit motifs in order to exercise our new analysis methods and to provide guidance for subsequent work on more complex component networks. Given the ubiquity of feedback configurations for noise suppression within microelectronic circuits, it seems natural to focus such preliminary exploration on coherent (optical) feedback motifs for managing quantum fluctuations in ultra-low power nanophotonic circuits.

Here we consider a coherent feedback strategy for suppressing spontaneous switching in dispersive optical bistability. Dispersive bistability is of interest as a potential physical basis for the design of ultra-low power nanophotonic switches, but in the attojoule switching regime where the logical states are separated by a small number of photons, quantum fluctuations will induce unwanted spontaneous switching that must be accounted for in circuit design. For example, **Fig. 1** shows a simple quantum trajectory simulation of the mean intracavity photon number for a Kerr-nonlinear optical resonator, assuming parameters that classically would be expected to support dispersive optical bistability with attojoule separation between the logical high and low

states. The quantum model clearly predicts spontaneous transitions that would compromise the performance of such a device in a photonic switching context.

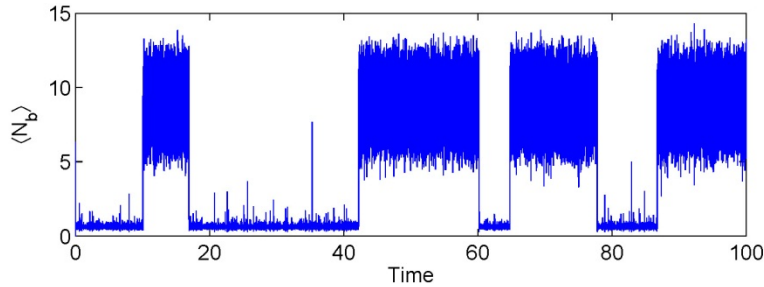


**Figure 1. Quantum trajectory simulation.**

In order to motivate our coherent-feedback stabilization strategy for suppression of such quantum jumps we first consider a feedback configuration with a linear static controller. If we assume that the bistable (plant) cavity has three distinct input-output ports corresponding to the bias input and the feedback-loop input and output, we can model the effects of a simple optical feedback loop with unit gain and total phase shift as depicted in the upper left panel of **Fig. 1**. The net effects of the feedback loop are a frequency pulling of the effective drive detuning and a change in the effective cavity decay rate. Either or both of these effects could potentially be used to suppress spontaneous switching of the bistable cavity if the feedback phase could be adjusted to a value that stabilizes the low state when the state is low, and to a value that stabilizes the high state when the state is high.

To realize the desired form of nonlinear dynamic controller we consider an auxiliary (controller) Kerr-nonlinear optical cavity connected as shown in the upper right panel of **Fig. 2**. As the Kerr nonlinearity causes the effective cavity detuning to vary with drive strength, such a cavity imparts a drive amplitude-dependent phase shift on the beam that reflects from its input coupler. The lower panel of **Fig. 2** shows an approximate representation of reflected phase versus drive amplitude. Our basic coherent control strategy is to set the overall feedback phase close to  $\pi$  when the plant is in the low photon-number state and closer to zero when the plant is in the high photon-number state.

The upper panel of **Fig. 3** displays a quantum trajectory simulation of the closed loop model; spontaneous transitions between low and high photon-number states are clearly still present but occur at a reduced rate. The lower panel of **Fig. 3** shows the complex phase of the plant and the phase of the coherent feedback field after reflection from the controller cavity on the same time axis (although significantly low-pass filtered to reduce shot-noise fluctuations). The difference of these two values corresponds to the phase shift of the coherent feedback loop. In accordance with the intuitive strategy described above, it can be seen that the feedback phase shift takes a value that decreases the effective plant decay rate when the plant is in the low photon-number state.

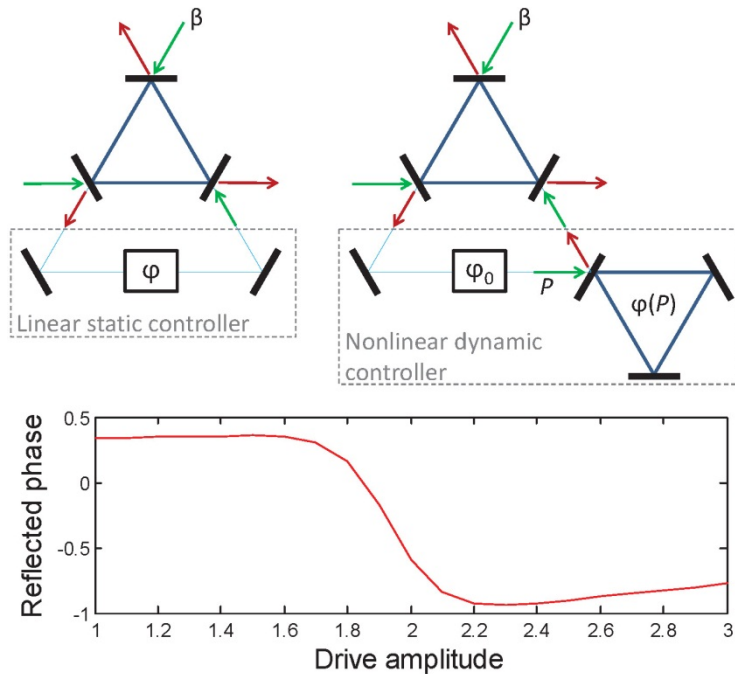


**Figure 2. Coherent feedback schemes.**

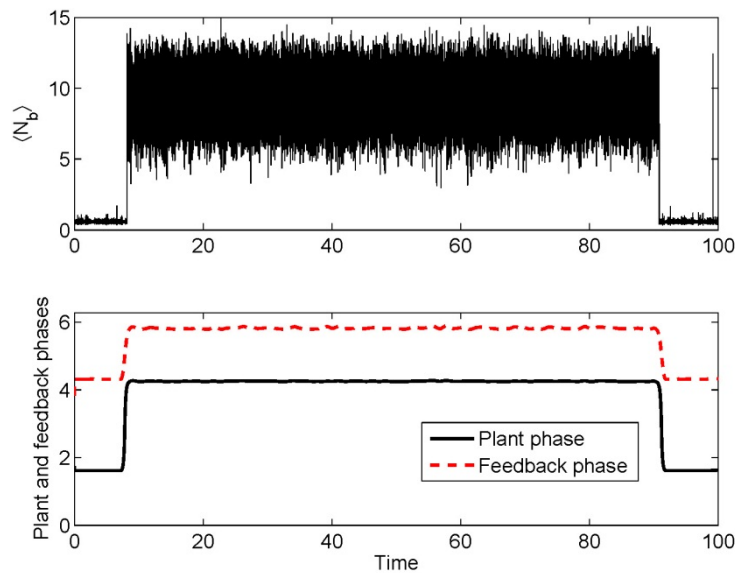


**Figure 3. Effects of coherent feedback.**

The inset of **Fig. 4** displays the evolution of the mean plant photon number as a function of time, starting from either a zero- or nine-photon initial condition (computed in the closed-loop cases by numerically integrating the master equation and in the open-loop case by numerical diagonalization of the Liouville super-operator). In the long time limit both initial conditions regress to a steady-state value, which is the average of the conditional mean photon number in the low and high logical states. Results are shown for the open-loop case and the dynamic coherent feedback cases. It can be seen that the low and high logical states, and therefore the steady-state photon number, vary

somewhat among the three cases. The main plot of **Fig. 4** displays the same data in a normalized fashion.

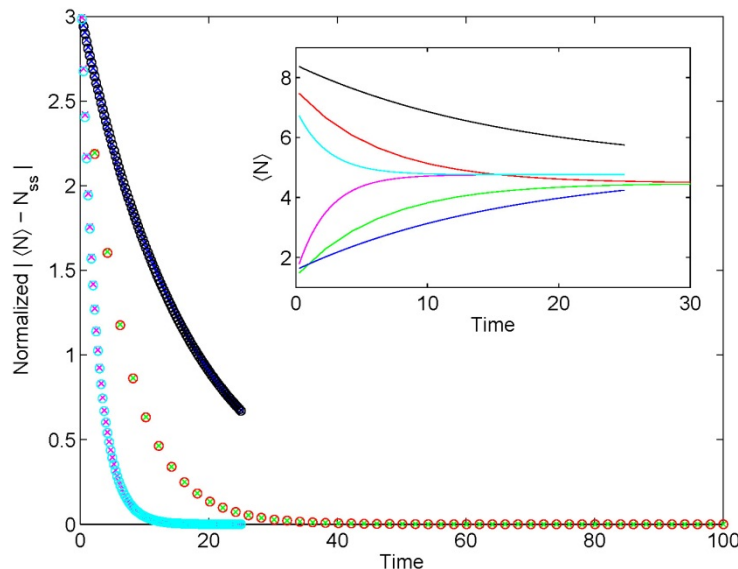


**Figure 4. Change in spontaneous switching rates.**

It should be noted that within the two-cavity coherent feedback configuration we have considered, and with the key structural parameters of the plant cavity held fixed, there remains a great deal of room for optimizing the operating conditions and controller parameters to achieve potentially superior suppression. Given the rather demanding nature of the numerical computations involved (a total Hilbert space dimension of 625 was used in this work and Master Equation integrations were essential), a brute-force scan of so many degrees of freedom would not seem feasible but it seems likely that a more principled computational optimization approach could be developed.

Recent theoretical investigations—based on classical electromagnetic models—of circuit motifs and optimal pulse shaping for switching applications have offered a glimpse of the great potential for innovative engineering at the signals-and-systems (as opposed to device physics) level in nanophotonics. Here we have attempted to extend this exploration to the quantum optical regime of attojoule switching energy, demonstrating theoretical methods that can be used to analyze intuitive coherent feedback control schemes in quantitative detail.

## 2.0 NONLINEAR INTERFEROMETRY APPROACH TO PHOTONIC LOGIC

Nanophotonic engineering has grown rapidly in recent years, fueled by remarkable advances in the fabrication of high quality-factor low mode-volume optical resonators. A number of research groups have begun to demonstrate the potential of such structures for enabling ultra-low energy (sub-fJ) optical switching based on the bulk nonlinearity of optical materials such as InGaAsP. Although large-scale integration of such nonlinear-resonator devices to form complex feedforward/feedback networks remains a formidable challenge, substantial progress is being made, making this an opportune moment to contemplate strategies for designing signal processing circuits that leverage unique physical attributes of the nanophotonic substrate.

Here I propose a high-level approach to photonic logic based on interferometry with nonlinear components, which exploits both the strong optical nonlinearities that may be obtained in high-Q/V resonators and the possibility of circuit-scale optical coherence (phase stability) that may be anticipated in monolithic nanophotonic circuits. Using a simple Kerr-type Hamiltonian to describe the cavity nonlinear optics, it is possible to derive quantum optical models for fundamental components such as a NAND gate (with fan-out) and a bistable latch. Such models can be interconnected using simple circuit algebra and are in fact compatible with a hardware description language-based schematic capture workflow for complex circuit design. Through numerical simulation it is possible to explore the impact of quantum fluctuations on the operation of compound devices such as the bistable latch, indicating a significant need to study circuit topologies that utilize coherent feedback to suppress quantum noise in classical ultra-low power photonic signal processing.

Signals in this logic scheme correspond to coherent states of single transverse-mode propagating electromagnetic fields, with complex amplitudes of zero and  $\alpha$  representing low and high signal levels. The diagrams in **Fig. 5** depict arrangements of optical components that realize a single-output AND gate (a) and a NOT gate with output fanout-of-two (b). Although discrete components are depicted, these are meant to stand for analogous arrangements of nanophotonic resonators, waveguides and splitters. The key element in each gate construction is a Kerr-nonlinear optical ring resonator (cavity) with two input-output ports.

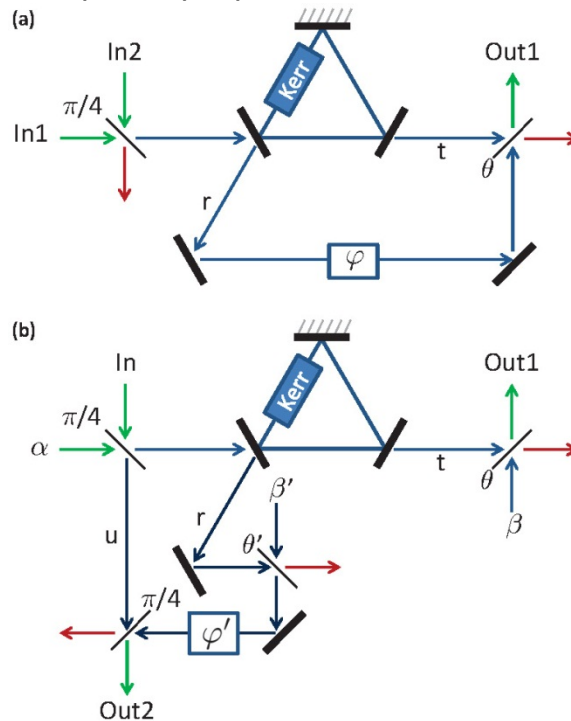


**Figure 5. Diagrams of AND, NOT gates.**

**Fig. 6(a)** shows the steady-state response of a Kerr-nonlinear cavity. The parameters are chosen here to obtain switching dynamics with stored energy in the range of tens of photons per cavity, which seems to represent the minimum operational energy scale that can be contemplated before quantum shot-noise fluctuations begin to

dominate the device physics. The horizontal axis corresponds to the input flux-amplitude and the vertical axis corresponds to the magnitude of the flux-amplitude of the transmitted field (black solid curve) or reflected field (dotted red). Threshold behavior associated with the Kerr nonlinearity, which can be exploited to drive logic operations, is clearly visible.

The single-output AND gate is configured with an input 50/50 beam-splitter that mixes the two input signals. Although there is some freedom in choosing a precise value for  $\alpha$ , here we use 22.6274 in order to push the low+high input level well below the response threshold and high+high above. With zero driving field the overall output of the gate is clearly zero, trivially satisfying one line of the truth table. The complex amplitudes of the transmitted (blue) and reflected (red) fields are indicated in **Fig. 6(b)**. Because of the dispersion in both the magnitudes and phases of these responses, it is possible to recombine the reflected and transmitted fields as indicated in **Fig. 5(a)** to ensure that the coherent mean of the output signal is nulled for low+high and high+low inputs while the output magnitude is at least  $\alpha$  for high+high inputs.

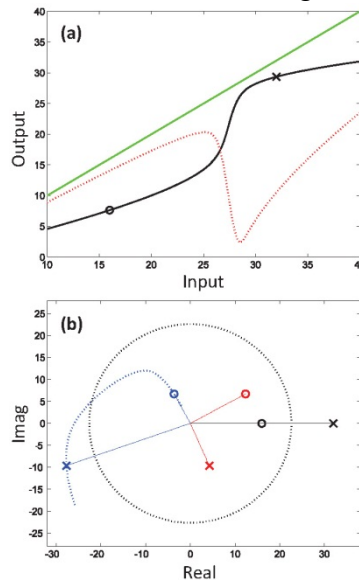


**Figure 6. Kerr nonlinearities.**

It should be noted that although the gate designs have been discussed here in terms of the coherent means of the signal fields, the cavity nonlinear dynamics do not quite preserve coherent states but rather induce small amounts of squeezing for the parameters chosen. In the ultra-low power regime (which requires strong Kerr nonlinearities) it is thus of substantial interest to study how such quantum effects propagate through a complex circuit and induce non-ideal behavior, but this is left for future studies based on more concrete implementation scenarios. Note also that Markov approximations are assumed in the cavity interactions with propagating signal fields, and that the propagation time delay between components is neglected (although arbitrary propagation phase-shifts can be included where desired).

In addition to combinatorial gates, the nonlinear interferometry approach admits sequential logic components such as a bistable latch. **Fig. 7** depicts one possible construction based on the feedback interconnection of two Kerr-nonlinear cavities, which operates in a manner analogous to that of a canonical SR-NAND latch in

electronics. The latch exhibits bistability in the photon numbers of the two cavities. A quantum-optical model corresponding to **Fig. 7** can be derived straightforwardly using series and concatenation products. As with the electronic SR-NAND latch, the HOLD condition for this device is both inputs high, while the condition with both inputs low leads to undefined response. The internal logical state of the latch (corresponding to high mean photon number in the first cavity and low mean photon number in the second, or vice versa) can be SET or RESET by pulling one input low with the other held high. The symmetric steady-state joint photon number distribution obtained with the HOLD input condition is shown in **Fig. 8(a)** and a quantum trajectory simulation of switching dynamics is shown in **Fig. 8(b)**. Numerical analysis reveals that in this ultra-low internal energy regime, such a latch exhibits spontaneous switching due to quantum fluctuations, and that the switching dynamics seem to be affected by a third metastable state (in addition to the two logical states) with equal photon number in the two cavities. Although the individual cavity decay rates potentially allow for output field changes on short timescales, the feedback dynamics apparently dictate longer switching times; pauses in the switching waveform are occasionally observed as the latch crosses through the equal photon-number condition resulting in increased switching times. It would of course be desirable to optimize the latch stability and switching by varying design parameters within the space of feasible values for any given concrete implementation.

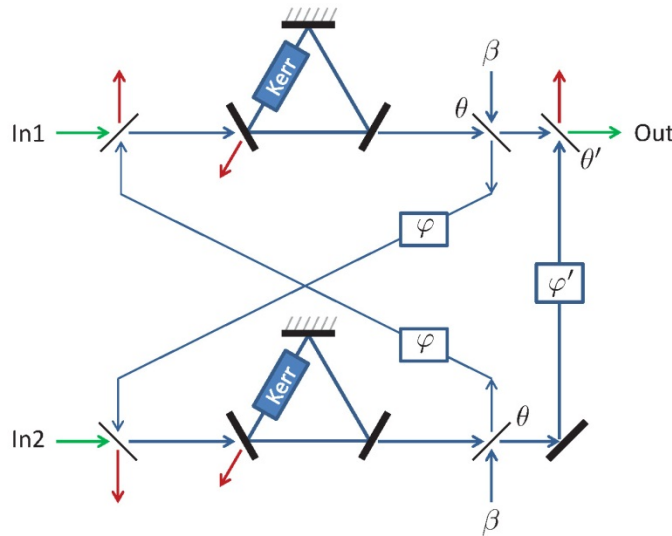


**Figure 7. Bistable latch diagram.**

The gate and latch designs presented above serve to illustrate the basic principles of a nonlinear interferometry approach to photonic logic, exploiting the complex input-output response of Kerr-nonlinear cavities (including both phase dispersion and thresholding behavior in the signal magnitudes to realize the required truth tables) as well as the circuit-scale phase stability that may be anticipated in monolithic nano-patterned structures. Given the importance of power minimization for future information processing technologies, it seems natural to work with quantum optical models for precise quantitative analysis of the impact of quantum fluctuations on stability and dynamic behavior in nanophotonic circuits operating in the few-photon

regime. Design studies that explore the performance, efficiency and robustness of candidate architectural approaches may provide crucial guidance for the continuing development of nanophotonic fabrication techniques and optical thin-film materials.

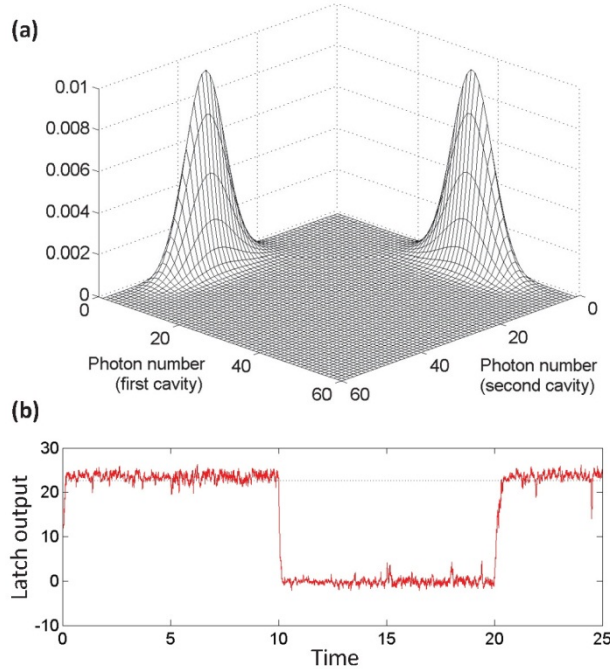


**Figure 8. Bistable behavior.**

### 3.0 QUANTUM REMNANTS OF BISTABILITY IN THE ATTOJOULE REGIME

Current approaches to high spatial-density, ultra-low power photonic switching utilize optical resonators with small mode-volume and high quality-factor to enhance the effective nonlinearity of bulk materials such as Si or InGaAsP. Such resonators likewise play a crucial role in cavity QED research with single emitters such as quantum dots or diamond nv-centers. Whereas atomic and solid-state cavity QED experiments are routinely analyzed using quantum models, research aimed towards switching applications typically employs classical electromagnetic methods to model nanophotonic versions of the bistability and hysteresis phenomena that have dominated optical computer engineering since the 1970s. Classical optical models are ultimately incompatible with the technological goal of low switching energy, however, as the characteristic scale of one attojoule corresponds to below ten photons at near-infrared wavelengths. Here we present experimental data on attojoule optical bistability that *clearly illustrate the significance of quantum-optical effects for switching-related nanophotonic device physics.*

Our experiment utilizes a single gas-phase atom as the nonlinear medium in a Fabry-Perot optical resonator, but the methods we use to analyze quantum effects in the data can be applied straightforwardly to solid-state systems. We characterize the dynamic input-output properties of the atom-cavity system in a parameter regime that would be expected, on the basis of semiclassical mean-field theory, to exhibit absorptive bistability with a hysteresis loop suitable for attojoule optical switching.

Theoretical studies have shown that quantum fluctuations of the cavity field and atomic dipole should induce spontaneous switching between the low- and high-transmission states, and thus destroy true optical bistability, when the energy separation of the semiclassical attractors is brought down to attojoule scale (tens of photons) through the use of a small mode-volume and high quality-factor resonator (except in the so-called good cavity limit, which is not relevant to nanophotonics). A previous experimental study of single-atom cavity QED in a similar parameter regime clearly demonstrated the validity of quantum (as opposed to semiclassical) methods for predicting steady-state observables, but here we take an important step further by recording dynamic signals that reveal the quantum ‘remnants’ of bistable behavior in the attojoule regime. Finding ways to functionalize such remnant behavior in the design of robust attojoule photonic switches is an outstanding challenge for quantum engineering.

The Maxwell-Bloch Equations (MBEs) represent a mean-field approximation to the quantum master equation for cavity QED in the limit of weak coupling and large atom number. They are semiclassical in the sense that they treat the atomic ensemble quantum mechanically but the field classically, and have been used extensively in prior research on optical bistability with atomic ensembles as the intracavity nonlinear medium. The MBEs can be written as a set of five real first-order differential equations and are amenable to analysis using the tools of dynamical systems theory. In single-atom cavity QED with strong coupling and strong driving fields, the MBEs retain some relevance as a sort of orthogonal projection of the quantum master equation onto the sub-manifold of semiclassical atom-field states (separable states with the field in a coherent state) and numerical studies have shown that solutions of the full quantum model often mimic those of the MBEs in some qualitative way.

The MBEs predict absorptive optical bistability for the parameters of our experiment, as shown in **Fig. 9(a)**. In this plot the vertical axis represents input drive amplitude, and as a function of drive strength the solution curve passes through horizontal planar coordinates corresponding to the real and imaginary parts of the steady-state complex field amplitude(s). A typical bistable structure appears with two stable solutions and one unstable solution co-existing over a range of drive strengths. The projection of the curve onto the bottom face of the 3D coordinate box helps to indicate the phases of the steady-state solutions, while the projection onto the back face illustrates the input-output relation that would be inferred by a measurement technique such as amplitude-quadrature homodyne detection. Using identical parameters, the steady-state solution of the quantum master equation can be determined for each value of the input drive strength and the marginal state of the cavity field can be obtained by tracing over the atomic degrees of freedom. Contours of the corresponding Wigner function (a quasi-probability distribution representation over complex amplitudes of the intracavity field) are displayed for a representative set of drive strength values in **Fig. 9(b)**. A double-peaked structure emerges in a range of drive strengths similar to the bistable region of the MBEs (and recurs at higher drive strengths, but this recurrence is understood to correspond to the onset of a distinct nonlinear dynamical phenomenon). The two peaks of this distribution may be associated with the low- and high-amplitude branches of the semiclassical bistability curve, but in the quantum model neither of them is truly stable. In any single experimental trial the cavity field (and thus the output power) will spontaneously switch

between low and high amplitude states, as shown in the experimental data of **Fig. 9(c)** (explained further below). Such stochastic switching is a dramatic consequence of quantum fluctuations in the attojoule regime and clearly must be taken into account in the design of practical switching devices.

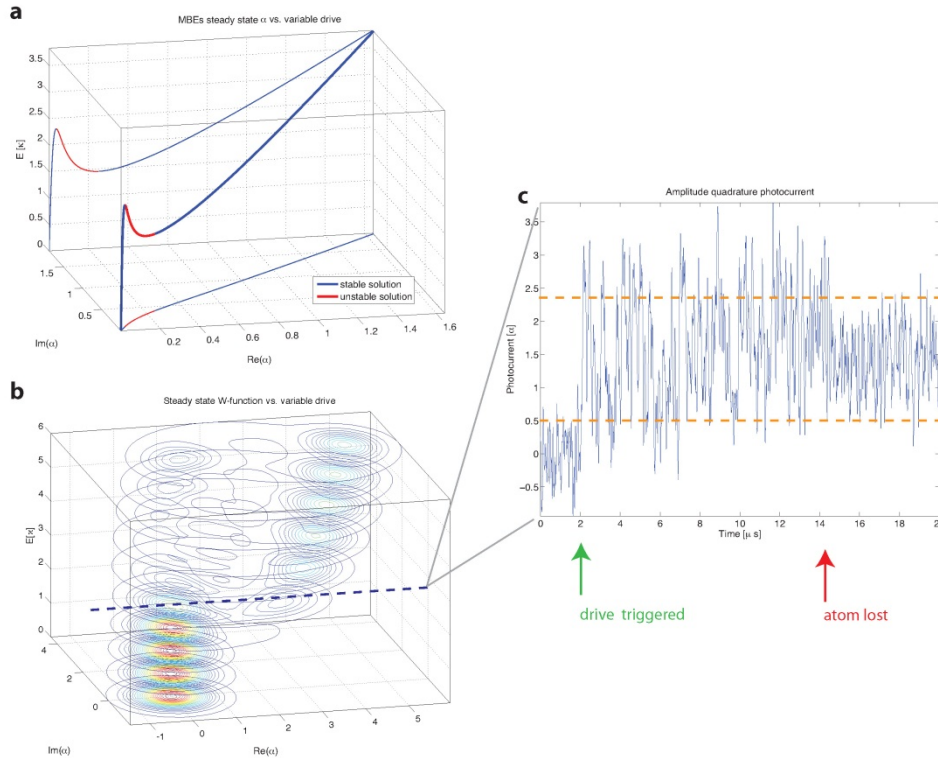


**Figure 9. Absorptive bistability in cavity QED.**

In our experiment, laser cooled Cs atoms are dropped into a high-finesse Fabry-Perot optical resonator supporting a circularly-polarized, 852nm TEM<sub>00</sub> mode actively stabilized at a precise frequency relative to an atomic cycling transition. As an individual atom falls through the cavity mode, it experiences a position-dependent coupling rate to the mode that is monitored by the transmission of a weak and detuned optical probe. Once a near-maximally coupled atom is detected, the probe strength is increased, the detuning from the atomic transition decreased and optical homodyne detection of a particular quadrature of the transmitted field is initiated (as happens at the time indicated by the first arrow on the time axis in **Fig. 9(c)**). With the drive amplitude held at a fixed value within the bistable/bimodal region, the amplitude quadrature of the transmitted field (i.e., the output field quadrature with the same phase as that of the driving field) is seen to switch stochastically between high and low states. Typically the atom-induced signal is lost after approximately 10 $\mu$ s, because the atom either exits the cavity mode or is pumped into a dark state, as signaled by the homodyne photocurrent settling rapidly to the mean value and gaussian noise level indicative of simple transmission through an empty cavity (as happens at the time indicated by the second arrow on the time axis in **Fig. 9(c)**).

In **Fig. 10** we compare photocurrent distributions (histograms of photocurrent segments, such as the segment between the ‘drive triggered’ and ‘atom lost’ events in **Fig. 9(c)**, along the vertical axis) obtained from multiple experiments with amplitude-

and phase-quadrature measurements for three different sets of mode-drive, atom-drive detunings and drive amplitudes. For a near-detuned system at the onset of bistability, wide/bimodal and narrow/normal distributions are apparent in the amplitude- and phase-quadrature distributions, respectively (**Fig. 10(a)**). However, when the atom-drive detuning is increased for the same drive amplitude, the low-amplitude transmitted field dominates (**Fig. 10(b)**). This imbalance reflects an increased drive threshold for the onset of bistability with larger detuning. Consequently, the bimodal amplitude distribution reemerges when the drive amplitude is increased in **Fig. 10(c)**. The data are in agreement with theoretical predictions based on a fully quantum-mechanical measurement model (using calibrated detection inefficiencies and bandwidths), despite the use of somewhat idealized models that assume a static coupling rate. A fixed effective value provides a good visual fit for all three parameter sets for data taken from the largest amplitude-quadrature switching segments. We believe that this approximation of fixed coupling and the finite (20 MHz) bandwidth of our presented homodyne signals account for slight mismatches between theory and experiment of the amplitude quadrature splitting and phase-quadrature mean in the three data sets.

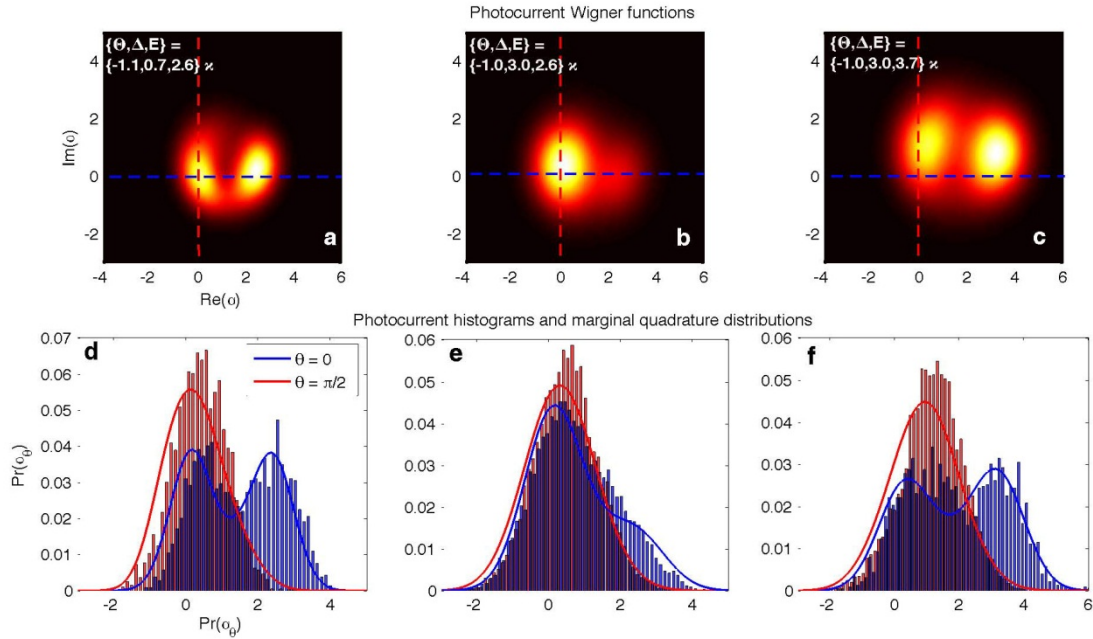


**Figure 10. Steady-state homodyne distributions.**

Hence, even in the attojoule regime, the distinct high- and low-amplitude states of the intracavity field are not washed out completely by quantum fluctuations. The remnant signatures of optical bistability are visible in the bimodal output photocurrents shown in **Fig. 10**, and also in a sort of ‘kinetic’ (as opposed to equilibrium) hysteresis that will be described below. We first establish from the photocurrent data that when an atom is present in the cavity, although the output field fluctuates strongly (between the high- and low-amplitude lobes of the bimodal distribution) it remains correlated over timescales much longer than that of light transmitted through an empty cavity (**Fig. 11**). This atom-induced memory effect can be seen as a quantum remnant of classical optical bistability, in which the high- and low-amplitude states are truly stable and would

therefore exhibit infinite correlation time. Consequently, it should still be possible to observe the hysteretic amplitude response characteristic of classical optical bistability by modulating the system drive slowly compared to the timescale for relaxation of the intracavity field (set in our case by the cavity decay time) but rapidly compared to the ‘metastable’ timescale indicated in **Fig. 11**. Following this idea, the data in **Fig. 12** were obtained by recording amplitude-quadrature homodyne photocurrents while sweeping the drive strength sinusoidally at 0.25MHz or 1MHz. **Figs. 12(a)** and **12(b)** depict representative single-shot photocurrent segments encompassing several cycles of sinusoidal drive amplitude modulation (AM) spanning the bimodal/bistable region. Increases in both the mean and variance of the output photocurrent, largely in phase with the drive amplitude, can be discerned in both of these real-time plots. However, plotting the photocurrent as a function of the instantaneous drive amplitude (**Figs. 12(c)** and **12(d)**) reveals a significant hysteresis in the system response at 1MHz AM that is barely noticeable at .25MHz. Whereas the response of the empty cavity is linear and non-hysteretic with fixed (shot-noise limited) output photocurrent variance at these modulation frequencies, nonlinear increases in the signal mean and variance are evident in both traces at mid-sweep. At 1MHz AM, a hysteresis loop appears to open between the upward and downward drive amplitude sweeps, with the low (high) state persisting over a wider range of increasing (decreasing) drive amplitudes than at .25MHz AM. These data are in agreement with theoretical predictions of the instantaneous photocurrent mean and variance computed using a fixed value of the coupling strength (as was also done for **Fig. 10**). We note that the slight elevation of the experimental high-amplitude branch in **Fig. 12(d)** relative to theory is consistent with the fixed-drive photocurrent histogram in **Fig. 11(d)**.

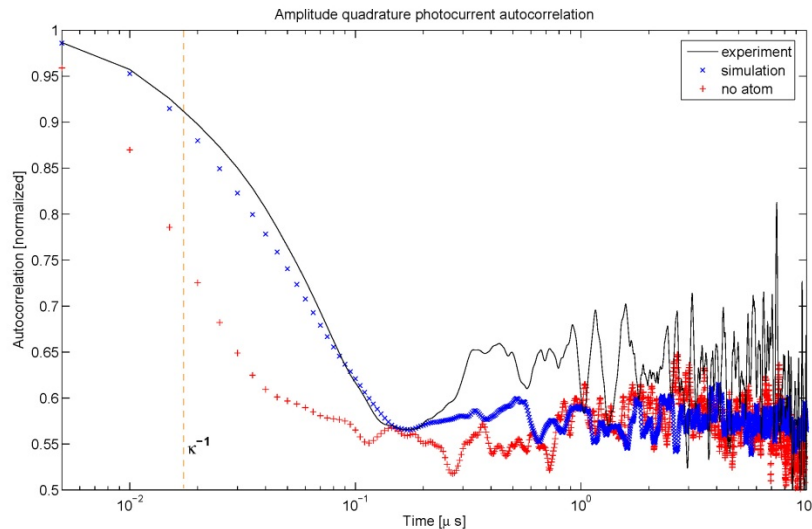


**Figure 11. Correlation functions.**

While the quantum fluctuation-limited lifetimes of the low- and high-amplitude states in attojoule optical ‘bistability’ may be too short for direct use in photonic switching, our results clearly illustrate that existing theoretical models are well suited to predicting and analyzing the dynamic response of real experimental devices. Such models can thus be used to make detailed predictions of the impact of quantum effects on ultra-low energy switch performance, and should be adopted more widely by the

photonic engineering community. Beyond mere simulation and analysis, we would emphasize that existing theoretical methods can and should be used to explore new engineering approaches to the suppression of quantum fluctuations in the design of switches and related nanophotonic devices, for example by exploiting embedded coherent feedback control. Even in a purely classical information processing paradigm, high spatial-density and ultra-low power nanophotonic circuit design presents intriguing new challenges for ***the nascent applied physics discipline of quantum engineering***.

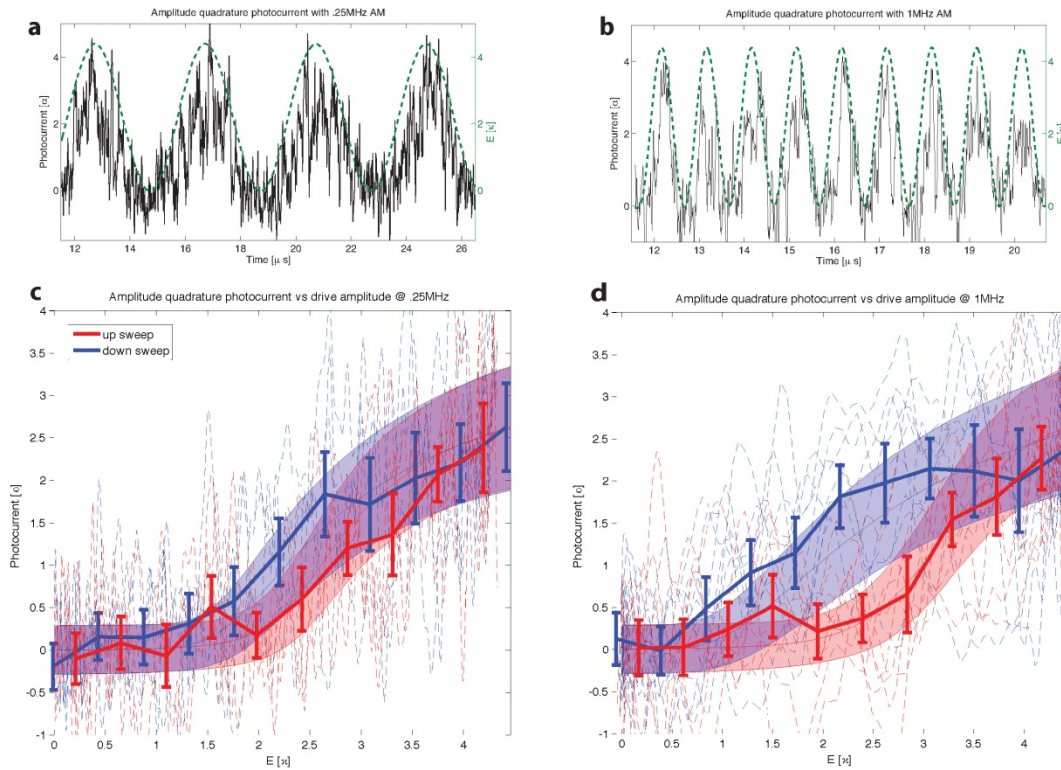


Figure 12. Hysteresis results.